

See discussions, stats, and author profiles for this publication at: <https://www.researchgate.net/publication/359010109>

# Research on Trenching Data Correction Method Based on Wavelet Denoising-Kalman Filtering Algorithm

Article in Arabian Journal for Science and Engineering · March 2022

DOI: 10.1007/s13369-022-06729-1

---

CITATIONS

2

READS

27

4 authors, including:



Xinzha Zhou

shihhezi university

6 PUBLICATIONS 9 CITATIONS

SEE PROFILE



# Research on Trenching Data Correction Method Based on Wavelet Denoising-Kalman Filtering Algorithm

Xinzha Zhou<sup>1,2</sup> · Za Kan<sup>1,2</sup> · Hewei Meng<sup>1,2</sup> · Yaping Li<sup>1</sup>

Received: 27 January 2021 / Accepted: 16 February 2022  
© King Fahd University of Petroleum & Minerals 2022

## Abstract

To realize monitoring of trenching depth, this paper built an online monitoring system and measured depth at three levels of 25 cm, 30 cm, and 35 cm. The test results show that the measured data have large fluctuations and low precision and are smaller than the actual value. For the above problems, this paper proposes a comprehensive noise reduction filtering algorithm based on wavelet noise reduction and Kalman filtering, in which the output of the preprocessing part of the wavelet noise reduction is used as the input of the postprocessing part of the Kalman filter. This article first selects the optimal combination of wavelet threshold denoising parameters such as wavelet function, decomposition level, and threshold denoising rule. Then the optimal Q/R value and the combination of Q and R parameters for the Kalman filter reprocessing part are explored. Finally, the comprehensive filtering correction algorithm and Kalman filtering algorithm are used to process the above-measured data. By comparing the results of the two algorithms, we found that for the local data, the variance decreased by 0.0207, 0.0398, and 0.0609, and the mean square deviation decreased by 0.0609, 0.0854, and 0.0457. The mean values of the two algorithms are very close. Similarly, for the global data, the variance decreased by 0.0182, 0.0549, 0.0428, and the mean square deviation decreased by 0.0359, 0.041, 0.0323. There is no significant difference in means between the two algorithms. The results show that the comprehensive algorithm improves the quality of trenching depth data and has certain significance for precision agriculture.

**Keywords** Agricultural machinery · Algorithms · Trenching depth · Wavelet denoising · Kalman filtering · Data correction

## 1 Introduction

With the continuous increase of fruit demand and orchard planting area, the orchard planting industry occupies an important position in agriculture [1]. According to statistics, the world's citrus fruit planting area in 2020 has reached 10,072,197 hectares [2]. Ditching is an important link in orchard management, which plays a decisive role in the follow-up fertilization and the quality of seedling planting. For example, the depth of the furrow determines the depth of

the fertilization layer. Different furrow depths will have different effects on fertilization quality. If the depth of furrow and fertilization is too shallow, it will affect the development of fruit tree roots. At the same time, it will also lead to the floating of fruit tree roots and low fertilizer absorption and utilization rate. If it is the opposite of the former, there will be a problem that the roots of fruit trees are difficult to absorb fertilizer, resulting in poor fertilization effect of fruit trees and excessive waste of fertilizer. In addition, due to the characteristics of large workload and short cycle time of trenching operation, mechanized trenching operation equipment and the impact of trenching operation on soil have also become key research topics in recent years [3–6], so as to meet the needs of modern orchard construction. To sum up, the depth of trenching is of great significance to the improvement of orchard soil, the growth of fruit trees, and the increase of yield, etc. [7–10]. Furthermore, it has an important impact on the quality of fertilization operations and fruit tree seedling planting and also provides the main basis

✉ Yaping Li  
shzz0527@126.com

Hewei Meng  
6318687@qq.com

<sup>1</sup> College of Mechanical and Electrical Engineering, Shihezi University, Shihezi 832000, China

<sup>2</sup> Engineering Research Center for Production Mechanization of Oasis Special Economic Crop, Ministry of Education, Shihezi 832000, China

for the optimization and improvement of related agricultural operation equipment.

Because of the importance of trenching depth in the process of agricultural machinery operation, scholars have researched relevant monitoring and control systems. At present, the main trenching depth monitoring methods are as follows: (1) a indirect measurement method based on angle sensors and displacement sensors, etc. [11, 12]; (2) a direct measurement method based on ultrasonic sensors [13]; and (3) a comprehensive measurement method that integrates the above two methods. For example, Wang et al. achieved real-time monitoring of tillage depth by applying two angle sensors to the electro-hydraulic control system [14]. S.M. Shafaei et al. monitored the current tillage depth through the potentiometer sensors and built a depth and traction control system based on fuzzy control to improve the tillage performance [15]. By connecting the moving wheel and the potentiometer on the plow, Soylu et al. finally realized the monitoring of tillage depth by building a model between the subsidence of the plow in the soil and the potentiometer [16]. The research of the above scholars further proves the necessity of trenching depth monitoring for the improvement of agricultural operation quality. Through the analysis, we can find that compared with the direct measurement method, when using indirect measurement to obtain the measurement data, it is necessary to analyze the geometric relationship of the tractor frame to realize the establishment of the tillage depth model. When this geometric relationship changes, the model needs to be re-analyzed and calibrated, which will bring some trouble to the user. Therefore, this paper adopts ultrasonic sensors to realize real-time monitoring of trenching depth.

Unfortunately, when monitoring systems are used, the signal measured by the sensor is inevitably interfered with by the noise signal, which leads to a decrease in the accuracy of the data. At present, many types of research are devoted to using the Kalman filter algorithm to denoise and correct measurement data. Quan et al. reduced the calculation error of acoustic transit time in the ultrasonic measurement of bolt stress by proposing an adaptive hybrid extended Kalman filter algorithm [17]. Ali Namdar et al. applied Kalman filter (KF) to the SITF detection algorithm, which improved the robustness and accuracy of the algorithm [18]. Jiang et al. developed a fault diagnosis method for drill string scour based on an iterative unscented Kalman filter and verified that the method can estimate the scour depth and scour rate within a certain noise range [19]. Hu et al. proposed an adaptive UKF method with process noise covariance estimation to enhance the robustness of the system to noise uncertainty [20]. Li et al. studied a fuzzy adaptive finite impulse response Kalman filter (FA-FIR-KF) algorithm, which improved the adaptive adjustment ability of the system to abnormal noise [21]. Through the above research, it is obvious that the correlation Kalman fil-

ter has a good effect on the noise reduction and correction of the signal. However, in the process of using the Kalman filter, it is assumed that the noise is Gaussian white noise, and the noise contained in the measurement data in the actual field ditching operation is more complicated. It is difficult to perfectly satisfy the assumptions of Kalman filtering, which reduces the quality of data noise reduction and correction, so it is necessary to preprocess the trenching depth data.

At present, due to its superior local noise reduction performance, wavelet noise reduction is widely used in agriculture [22–25], industrial damage and fault detection [26, 27], medical and biological signal monitoring [28–30], information prediction [31] and many other fields. Research in related fields shows that wavelet denoising algorithm not only retains the original characteristics of the signal, but also removes the noise signal. Therefore, the wavelet noise reduction algorithm is used as the preprocessing part of this comprehensive algorithm. Through wavelet noise reduction preprocessing on the trenching depth data, and linkage correction with the Kalman filter algorithm, the quality of trenching depth data is finally improved. Therefore, this paper applies the wavelet noise reduction algorithm as the preprocessing part of the comprehensive algorithm. By performing wavelet noise reduction preprocessing on the trenching depth data and then performing linkage correction with the Kalman filter algorithm, the quality of the trenching depth data is finally improved.

The rest of the paper is organized as follows: Sect. 2 describes the trench depth online monitoring system and the dataset. Section 3 describes the method proposed. Section 4 analyzes the parameter selection and optimal combination of wavelet denoising preprocessing part suitable for trenching depth to complete data preprocessing. Section 5 describes the Kalman filter reprocessing part, confirms the optimal Q, R values, and completes the Kalman filter reprocessing of the data. Section 6 applies the comprehensive noise reduction and correction algorithm proposed in this paper and analyzes the results in detail. Finally, in the seventh section, the conclusions and future directions of the study are presented.

## 2 Design and Data Collection of Trenching Depth Online Monitoring System

### 2.1 Design of Online Monitoring System for Trenching Depth

The trenching depth online monitoring system is mainly composed of the lower computer data acquisition system, the serial communication module, the upper computer data analysis system, and the access database. The schematic diagram of the system structure is shown in Fig. 1.



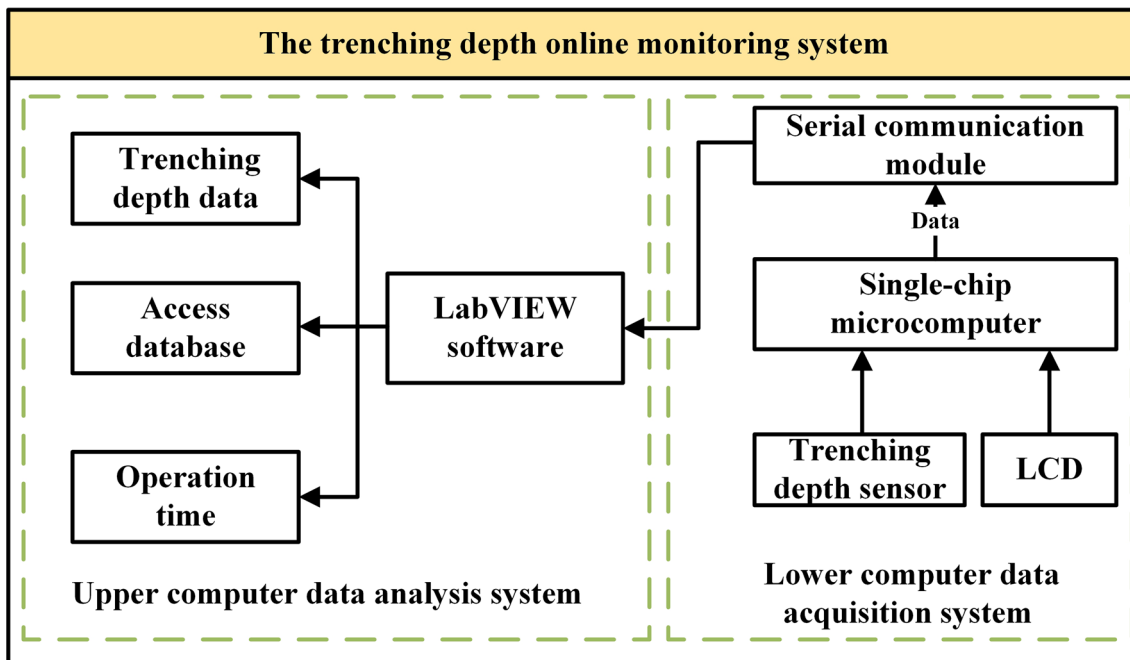


**Fig. 1** The schematic diagram of the system structure

The lower computer data acquisition system mainly realizes the acquisition function of trenching depth data, including a single-chip microcomputer, trenching depth sensor, LCD liquid crystal display, and other parts. The trenching depth sensor uses an ultrasonic sensor to collect trenching depth in real-time. The single-chip microcomputer analyzes and processes the trenching depth data collected in real-time, and displays the relevant data on the LCD liquid crystal display. The serial communication module takes the MAX232 chip as the core to realize the communication between the lower computer data acquisition system and the upper computer data analysis system. LabVIEW software is used in the data analysis system of the upper computer to build a user interface, which realizes the visualization and analysis functions of real-time data, and saves the data in the Access database.

## 2.2 Data Collection

The field test was carried out on the soil tank test bench, and the trenching depth data at three levels of 25 cm, 30 cm, and 35 cm were collected through the trenching depth online monitoring system, and the data was stored in the Access database. The total sample data points selected for each group of experimental data are 220. At the same time, this paper sets the total sample data as the global data and sets the data selected in the global data as the local data. Two kinds of data are processed using the comprehensive denoising algorithm to verify the denoising performance of the algorithm both locally and globally. The original data are shown in Fig. 2a,

b and c, where the selected local data are in the orange rectangle. Table 1 shows the calculation results of parameters such as the mean, variance, and standard deviation of the two kinds of raw data, and the comparison of their parameters is shown in Fig. 2d.

Combining the table and image, it can be found that the measured data fluctuates violently, and most of the data are smaller than the actual value of the trenching depth. Whether it's local data or global data, as the depth increases, the deviation between the data means and the current depth level becomes larger and larger, and the corresponding data variance and standard deviation also increase step by step. And compared with the local data, the variance and standard deviation of the global data are higher than those of the local data due to the more violent fluctuation of the global data.

Combined with the research of relevant scholars on the influence of operating environmental factors (temperature, soil moisture content, etc.) and soil characteristics on the ultrasonic sound velocity [32, 33], it is speculated that the primary sources of those problems may be: During data measurement, the data are affected by elements such as machine vibration, soil flatness, and operating environment, resulting in the interference of clutter and noise in the ultrasonic reflected signal, which reduces the accuracy of the measurement data.

To sum up, if the original measurement data is directly used for evaluating the quality of trenching operations, or for depth control of trenching operations of equipment, it will badly affect the performance of the system and the normal use of the equipment.



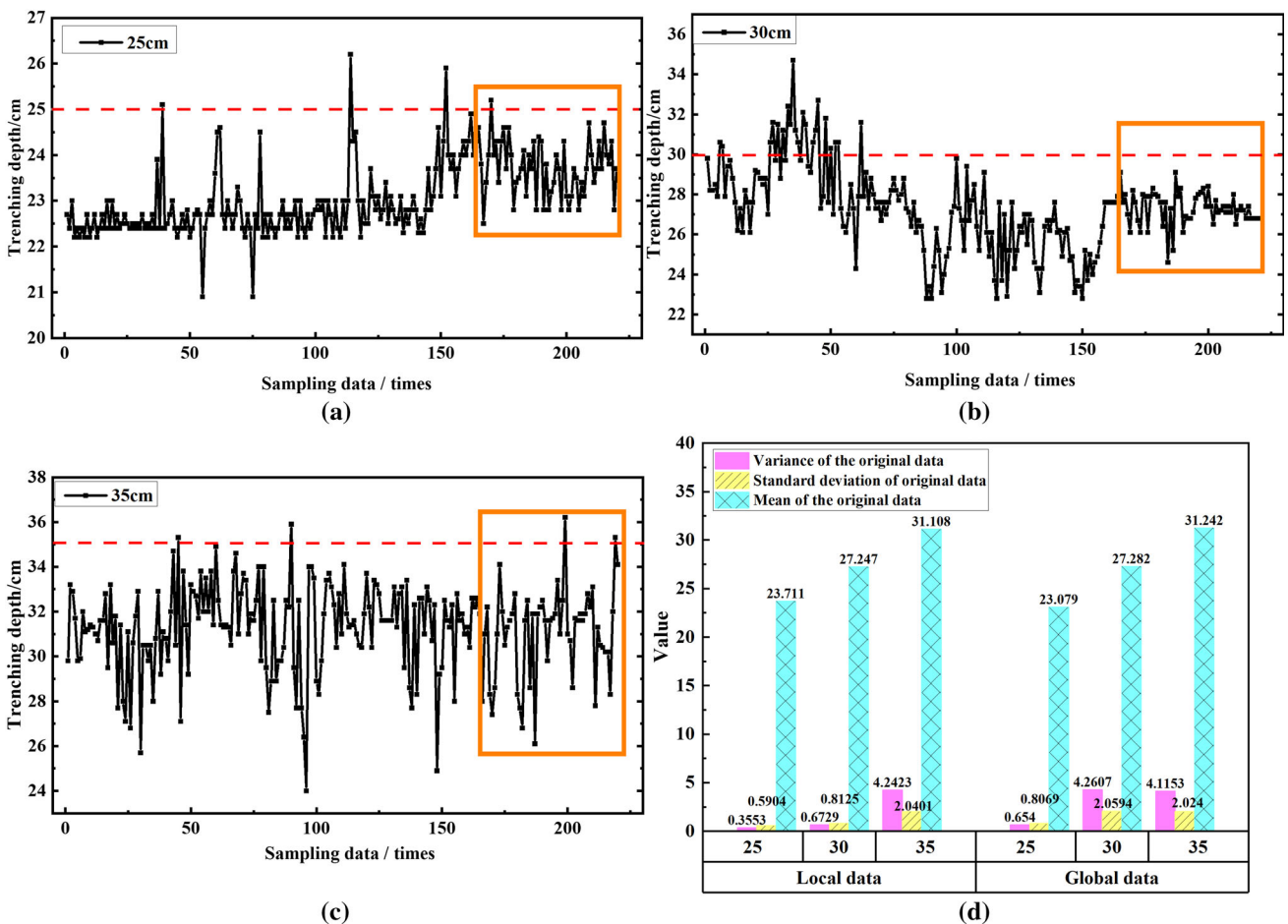


**Fig. 2** Original data and its parameters

**Table 1** The mean, variance, and standard deviation of the original data

Depth level/cm	Mean of the original data		Variance of the original data		Standard deviation of original data	
	Local data	Global data	Local data	Global data	Local data	Global data
25	23.711	23.079	0.3553	0.6540	0.5904	0.8069
30	27.247	27.282	0.6729	4.2607	0.8125	2.0594
35	31.108	31.242	4.2423	4.1153	2.0401	2.0240

So as to improve the reliability of trenching depth measurement data and provide accurate data sources for trenching operation quality identification and machine control, it is necessary to modify the original measurement data to meet the needs of practical application.

### 3 Composition of Algorithm

Aiming at the problems depicted in Sect. 2, this paper will combine the characteristics of trenching depth data, and propose a comprehensive filtering algorithm based on wavelet denoising and Kalman to correct the data. The method proposed in this paper for enhancing the accuracy of trenching

depth is described below. The corresponding flowchart is depicted in Fig. 3. The original measurement data are pre-processed by the wavelet noise reduction preprocessing part to distinguish and eliminate the noise data as much as possible, and through this way to finally improve the quality of the measurement data. Then, the Kalman filter reprocessing part takes the processed data as the input information, and further processes the data to realize comprehensive filtering and correction.

The preprocessing part of wavelet noise reduction is mainly divided into four parts: (1) option of evaluation parameters of wavelet noise reduction performance; (2) selection of optimal wavelet function; (3) determination of decomposition level; and (4) determination of noise reduc-



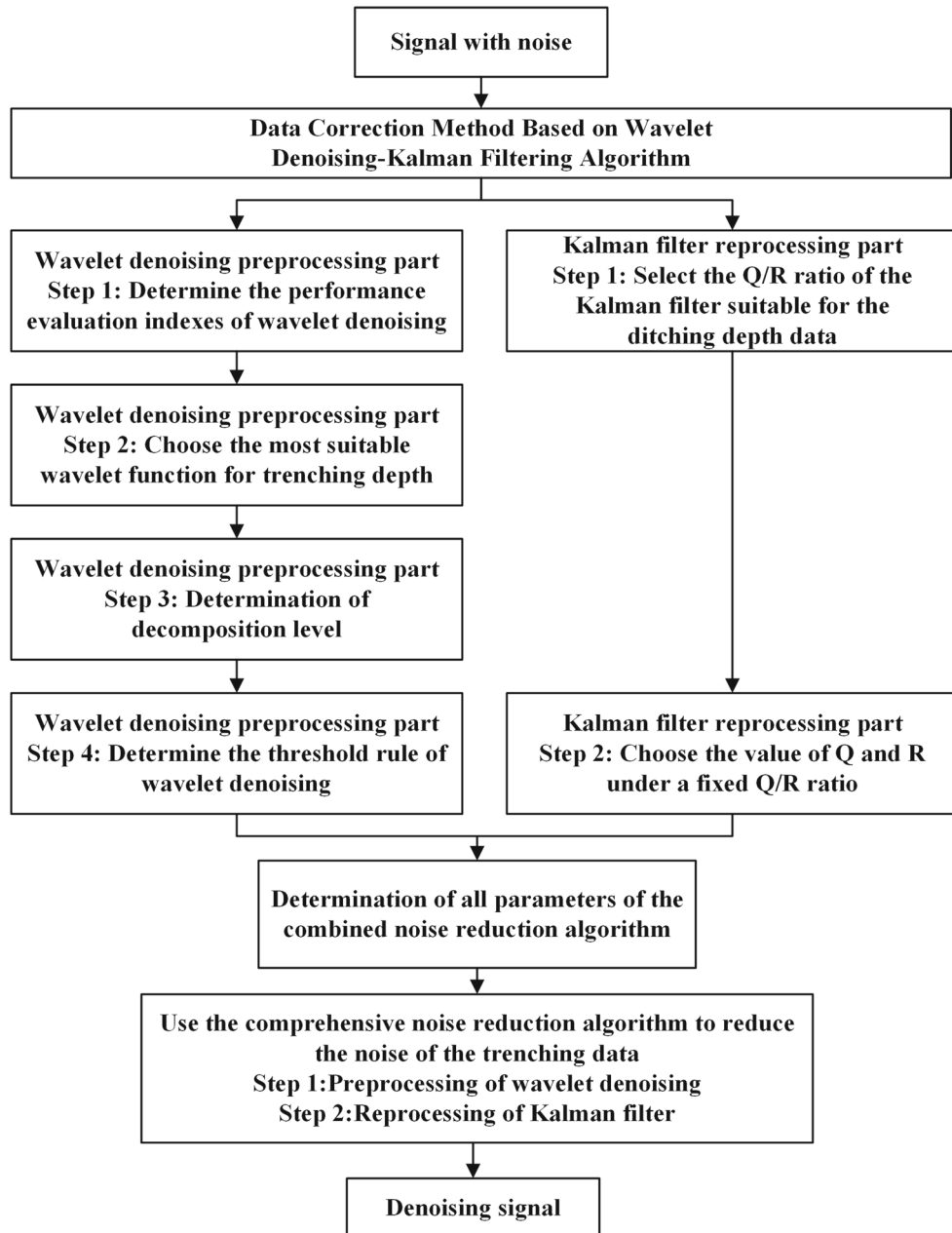


**Fig. 3** Flowchart of the process

tion threshold rules. The reprocessing part of the Kalman filter is mainly divided into two parts: (1) select the ratio of Q/R value, and (2) under the fixed ratio of Q/R value, select the parameter values of Q and R.

distinguish the clean signal from the noise signal as much as possible and finally retain the actual signal to realize the acquisition of noise-free signals. The model of one-dimensional noise-containing signals is as follows:

$$s(t) = f(t) + n(t) \quad (1)$$

Where  $s(t)$  is original signal,  $f(t)$  is the real signal, and  $n(t)$  is the noise signal.

The wavelet threshold denoising method used in this paper is to decompose the original signal by applying discrete wavelet transform (DWT) to obtain different wavelet coeffi-

#### 4 Wavelet noise reduction preprocessing part

Generally, the original signal is composed of an actual signal and a noise signal. The purpose of noise reduction is to



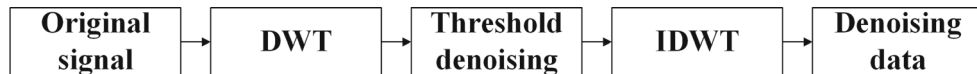


**Fig. 4** Wavelet threshold noise reduction processing flow chart

cients [31]. At the same time, according to the principle that the effective signal coefficient and the noise coefficient in the wavelet decomposition coefficients have different properties, they are processed and distinguished by selecting the appropriate threshold. Wavelet coefficients larger than the threshold value are preserved, if not, they are abolished. Finally, a new denoised signal is obtained by performing inverse discrete wavelet transform (IDWT) on the remaining wavelet coefficients [34], and the process is shown in Fig. 4.

#### 4.1 Performance Evaluation Metrics

To evaluate the performance of the noise reduction process, this paper mainly consists of three evaluation indicators: signal-to-noise ratio (SNR), root mean square error (RMSE), and correlation coefficient ( $\rho$ ) [35, 36]. The calculation formulas of the three evaluation indicators are as follows.

The SNR can be denoted as follows:

$$SNR = 10 \lg \left[ \sum_{i=1}^N s^2(i) / \sum_{i=1}^N (s(i) - \hat{s}(i))^2 \right] \quad (2)$$

The RMSE can be denoted as follows:

$$RMSE = \sqrt{\frac{1}{N} \sum_{i=1}^N (s(i) - \hat{s}(i))^2} \quad (3)$$

The  $\rho$  can be denoted as follows:

$$\rho = \frac{N \sum_{i=1}^N s(i)\hat{s}(i) - \sum_{i=1}^N s(i) \sum_{i=1}^N \hat{s}(i)}{\sqrt{N \sum_{i=1}^N s^2(i) - \left( \sum_{i=1}^N s(i) \right)^2} \sqrt{N \sum_{i=1}^N \hat{s}^2(i) - \left( \sum_{i=1}^N \hat{s}(i) \right)^2}} \quad (4)$$

where  $s(i)$  is the original signal,  $\hat{s}(i)$  is the denoised signal, and  $N$  is the signal length.

If the SNR is larger, the signal after noise reduction is closer to the real signal, and the noise reduction effect is better. If the RMSE is smaller, the deviation between the noise reduction signal and the actual signal is smaller, and the smoothness of the signal is better. If the value of  $\rho$  is closer to 1, the similarity between the noise reduction signal and the actual signal is higher.

**Table 2** Performance evaluation indexes results after denoising with dbN wavelet function

Wavelet function	db1	db2	db3	db4	db5
SNR	12.5930	13.6231	14.0746	13.2027	16.2326
RMSE	1.8091	1.6068	1.5254	1.6865	1.1898
$\rho$	0.9721	0.9781	0.9802	0.9758	0.9881
Wavelet function	db6	db7	db8	db9	db10
SNR	13.3324	9.0115	12.9250	21.2961	19.3680
RMSE	1.6615	2.7324	1.7413	0.6642	0.8293
$\rho$	0.9765	0.9351	0.9742	0.9963	0.9942

#### 4.2 Selection of Wavelet Function

In the process of signal denoising, the choice of wavelet function has a great influence on the denoising performance of the algorithm. Different wavelet bases have different time–frequency characteristics, so different wavelet base functions will produce different effects in the noise reduction process of the same signal. Considering the similarity, smoothness, and other factors of wavelet functions comprehensively, Daubechies (dbN), Symlets (symN), and Coiflets (coifN) wavelet families are selected to denoise the sampled data. According to the three evaluation parameters described in Sect. 4.1, the wavelet basis function most suitable for trenching depth data is selected.

In order to achieve the above purpose, this paper takes another group of trenching depth data as the sample data in this subsection and uses the fixed variable method to select the wavelet function. In this section, the parameters are set to four-level wavelet decomposition, hard threshold function, and Rigrsure threshold rule. The noise reduction effects of the above four families of wavelet functions are compared by MATLAB software, and the calculation results of the corresponding evaluation indicators are shown in Tables 2, 3 and 4.

It can be seen from Tables 2, 3 and 4 that when the wavelet functions of the dbN and symN series denoise the data, the SNR and  $\rho$  show a trend of first increasing, then decreasing, and then increasing as the order N increases. On the contrary, the RMSE showed a trend of first decreasing, then increasing, and then decreasing. Therefore, for the dbN and symN series of wavelet functions, the high-order denoising effect is better than the low-order denoising effect. For the coifN series of wavelet functions, as the order N increases, SNR and  $\rho$  first increase and then decrease, while RMSE decreases and then

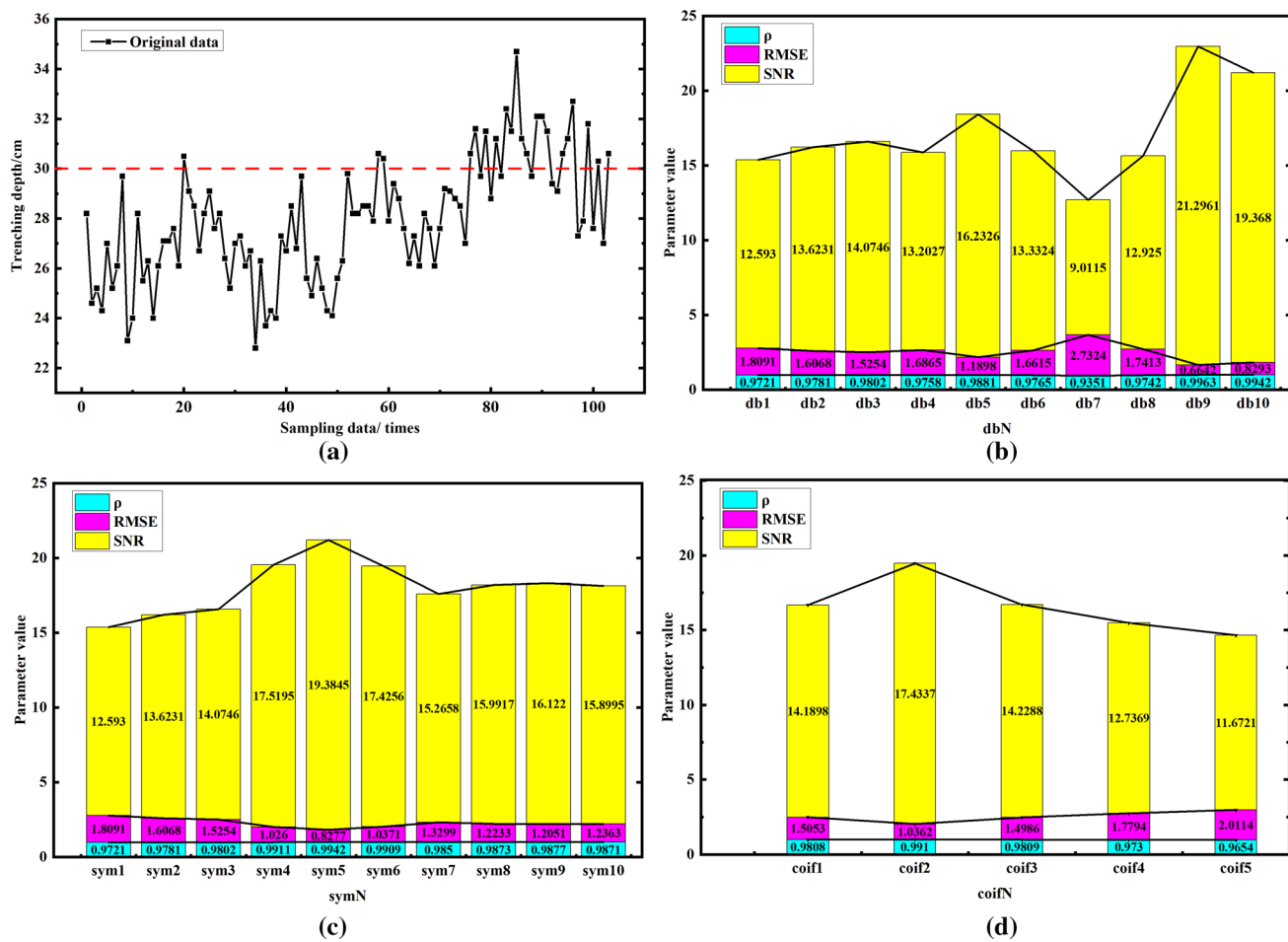


**Table 3** Performance evaluation indexes results after denoising with symN wavelet function

Wavelet function	sym1	sym2	sym3	sym4	sym5
SNR	12.5930	13.6231	14.0746	17.5195	19.3845
RMSE	1.8091	1.6068	1.5254	1.0260	0.8277
$\rho$	0.9721	0.9781	0.9802	0.9911	0.9942
Wavelet function	sym6	sym7	sym8	sym9	sym10
SNR	17.4256	15.2658	15.9917	16.1220	15.8995
RMSE	1.0371	1.3299	1.2233	1.2051	1.2363
$\rho$	0.9909	0.9850	0.9873	0.9877	0.9871

**Table 4** Performance evaluation indexes results after denoising with symN wavelet function

Wavelet function	coif1	coif2	coif3	coif4	coif5
SNR	14.1898	17.4337	14.2288	12.7369	11.6721
RMSE	1.5053	1.0362	1.4986	1.7794	2.0114
$\rho$	0.9808	0.9910	0.9809	0.9730	0.9654

**Fig. 5** The evaluation indexes of the three wavelet functions

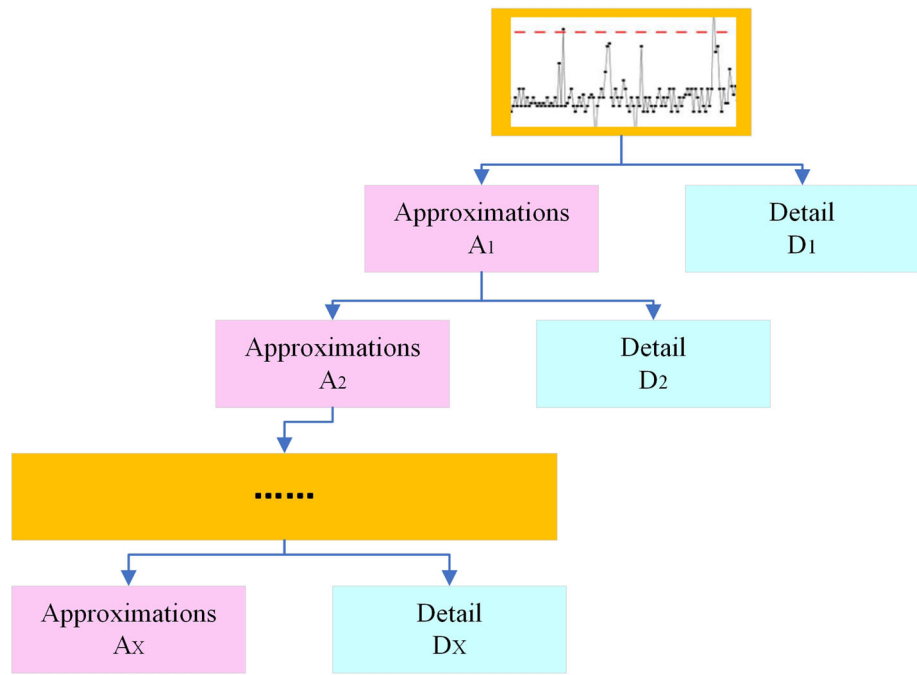
increases. Therefore, for the coifN series of wavelet functions, the denoising effect of low-order wavelets is better. The evaluation indexes of the three wavelet functions are shown in Fig. 5.

As can be seen in Fig. 5, it can be found that among the above three series of wavelet functions, the overall noise reduction performance of the dbN series wavelet functions and the symN series wavelet functions are relatively close, and the processing effects are mostly better than that of the coifN series wavelet functions. Comparing all the evaluation parameters comprehensively, seven wavelet functions, such as db5, db9, db10, sym4, sym5, sym6, and coif2, obviously have better noise reduction performance for trenching depth data.

Based on these seven wavelet functions, we explore the noise reduction performance under different decomposition levels and finally determine the optimal decomposition level, which will be shown in the next section.



**Fig. 6** Schematic diagram of wavelet decomposition



#### 4.3 Determination of Decomposition Levels

Figure 6 shows a schematic diagram of the signal decomposition of the wavelet algorithm. First, the noisy data is decomposed into approximations A1 and detail D1. Then the approximation A1 is decomposed into approximations A2 and detail D2. By analogy, the approximate value AX decomposed at each level will be decomposed into approximation coefficients and detail coefficients at the next level, until it is decomposed into the selected N layers.

In addition, if the decomposition level is too small, its calculation amount is low, but there will be problems of insufficient noise reduction performance and incomplete noise removal. If the decomposition level is too high, although the signal will be smoother, unfortunately, part of the valid signal will also be regarded as a noise signal. Therefore, the choice of the decomposition level also has a significant impact on the performance of the noise reduction algorithm.

To choose the best combination between the wavelet decomposition level and the wavelet function, the range of the decomposition level is set to 1–8 based on the Rigrsure thresholding rule. This section explores the noise reduction performance of seven wavelet basis functions, including db5, db9, db10, sym4, sym5, sym6, and coif2, at different decomposition levels.

Figure 7 shows the noise reduction performance, where the X-axis represents each wavelet basis function, the Y-axis represents the wavelet decomposition level, and the Z-axis represents the value of each evaluation index. The figure is divided into three lines, each line from top to bottom rep-

resents the SNR,  $\rho$ , and RMSE values of seven wavelet functions at different decomposition levels. By analyzing the surface graphs in the left column, it can be found that with the increase of the decomposition level, the values of SNR and  $\rho$  gradually decrease, while the RMSE gradually increases. At the same time, the trend of increase and decrease of the three evaluation indicators also changed from rapid to slow. The phenomenon in the histograms in the right column is that, from the perspective of the decomposition level, when the level is greater than 4 and 5 layers, the values of the three evaluation indicators no longer change significantly. Therefore, the optimal number of decomposition layers will be selected among 4 and 5 layers. From the aspect of the wavelet function, the overall noise reduction performance of sym5, db9, and db10 is better.

The detailed performance evaluation parameters are shown in Table 5.

By analyzing the data in Table 5, it can be concluded that when the decomposition level is 4 or 5, the noise reduction performance of db9 and db10 is better. By comprehensively comparing and considering the calculation amount and noise reduction performance of the wavelet noise reduction pre-processing part, we choose the optimal decomposition level as 4 and the optimal wavelet function as db9.

#### 4.4 Threshold Rules Selection for Wavelet Denoising

From the previous description, we can know that choosing a suitable thresholding rule is of great significance to the wavelet denoising performance. In this subsection, we will



**Table 5** Evaluation parameters results after denoising at different decomposition levels

Wavelet function	db5				db9				db10				sym4			
	RMSE	SNR	$\rho$	RMSE	SNR	$\rho$										
Wavelet decomposition level																
1	0.5854	22.3936	0.9971	0.3067	28.0072	0.9992	0.4031	25.6335	0.9986	0.3628	26.5482	0.9989	0.9998	0.9999	0.9999	
2	0.9948	17.7878	0.9916	0.4600	24.4866	0.9982	0.4979	23.7993	0.9979	0.8521	19.1329	0.9939	0.9939	0.9939	0.9939	
3	1.1778	16.3207	0.9883	0.6563	21.4007	0.9964	0.7816	19.8824	0.9949	0.9875	17.8516	0.9918	0.9918	0.9918	0.9918	
4	1.1898	16.2326	0.9881	0.6642	21.2961	0.9963	0.8293	19.3680	0.9942	1.0260	17.5192	0.9911	0.9911	0.9911	0.9911	
5	1.2046	16.1257	0.9878	0.8677	18.9753	0.9937	0.8315	19.3453	0.9942	1.0265	17.5148	0.9911	0.9911	0.9911	0.9911	
6	1.2041	16.1293	0.9878	0.8769	18.8828	0.9936	0.8313	19.3466	0.9942	1.0268	17.5123	0.9911	0.9911	0.9911	0.9911	
7	1.2040	16.1296	0.9878	0.8767	18.8852	0.9936	0.8349	19.3099	0.9942	1.0268	17.5123	0.9911	0.9911	0.9911	0.9911	
8	1.2035	16.1331	0.9878	0.8766	18.8864	0.9936	0.8348	19.3101	0.9942	1.0268	17.5123	0.9911	0.9911	0.9911	0.9911	
Wavelet function																
1	0.5074	23.6354	0.9978	0.5291	23.2710	0.9976	0.8991	18.6661	0.9932	0.8260	19.4030	0.9942	0.9942	0.9942	0.9942	
2	0.8028	19.6499	0.9946	0.7860	19.8336	0.9948	1.2502	15.8030	0.9868	0.8396	19.2608	0.9941	0.9941	0.9941	0.9941	
3	0.8168	19.5000	0.9944	1.0433	17.3738	0.9908	1.3295	15.2686	0.9850	1.0315	17.4727	0.9910	0.9910	0.9910	0.9910	
4	0.8277	19.3845	0.9942	1.0371	17.4256	0.9909	1.3299	15.2658	0.9850	1.0362	17.4337	0.9910	0.9910	0.9910	0.9910	
5	0.8359	19.2988	0.9941	1.0420	17.3852	0.9909	1.5068	14.1813	0.9808	1.0396	17.4048	0.9909	0.9909	0.9909	0.9909	
6	0.8434	19.2218	0.9940	1.0420	17.3846	0.9909	1.5104	14.1605	0.9807	1.0435	17.3726	0.9908	0.9908	0.9908	0.9908	
7	0.8434	19.2218	0.9940	1.0443	17.3654	0.9909	1.5099	14.1635	0.9807	1.0534	17.2900	0.9907	0.9907	0.9907	0.9907	
8	0.8448	19.2076	0.9940	1.3602	15.0704	0.9909	1.5099	14.1631	0.9807	1.0544	17.2824	0.9907	0.9907	0.9907	0.9907	



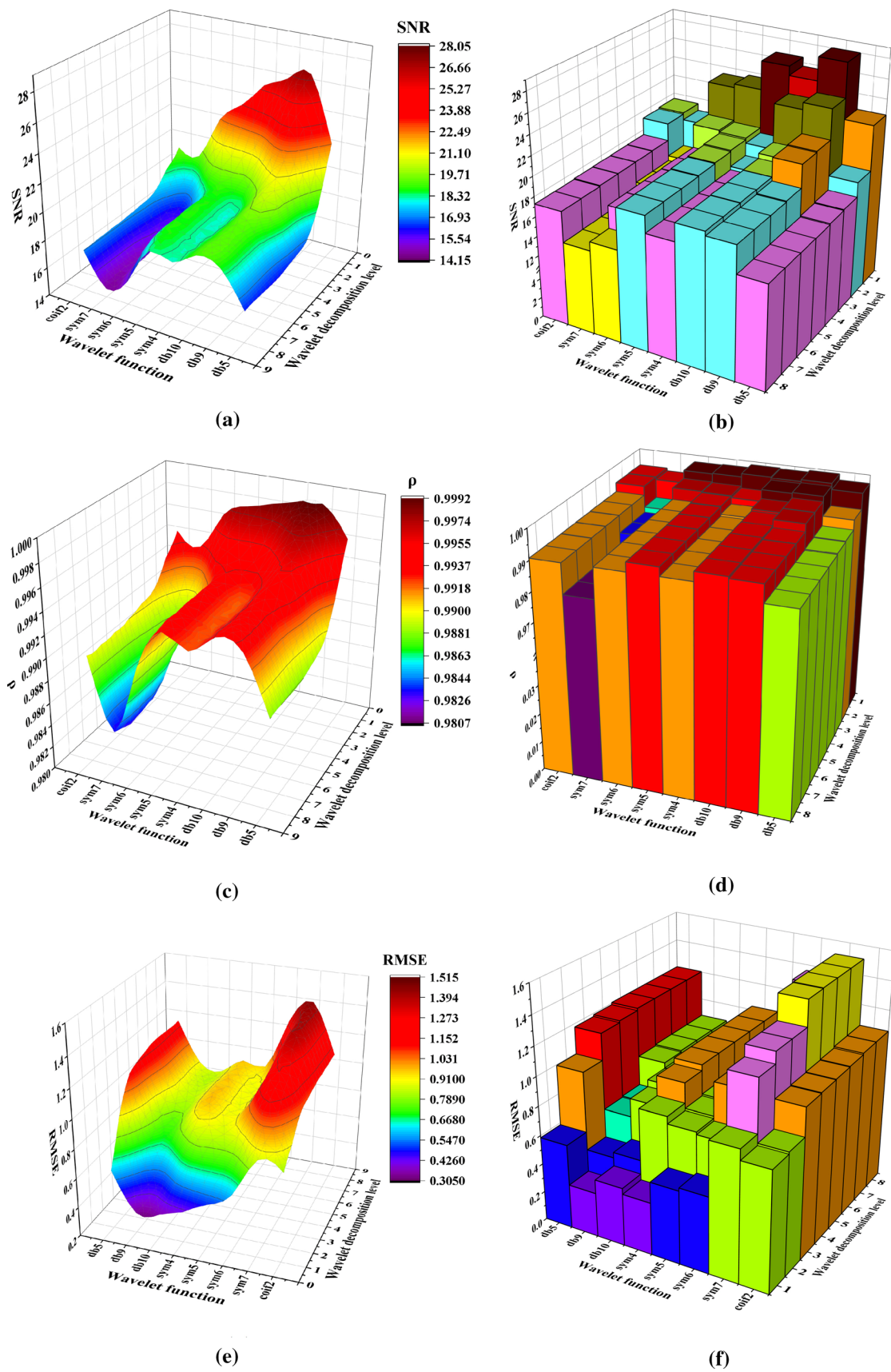


**Fig. 7** Schematic diagram of noise reduction performance under different decomposition levels and wavelet function combinations

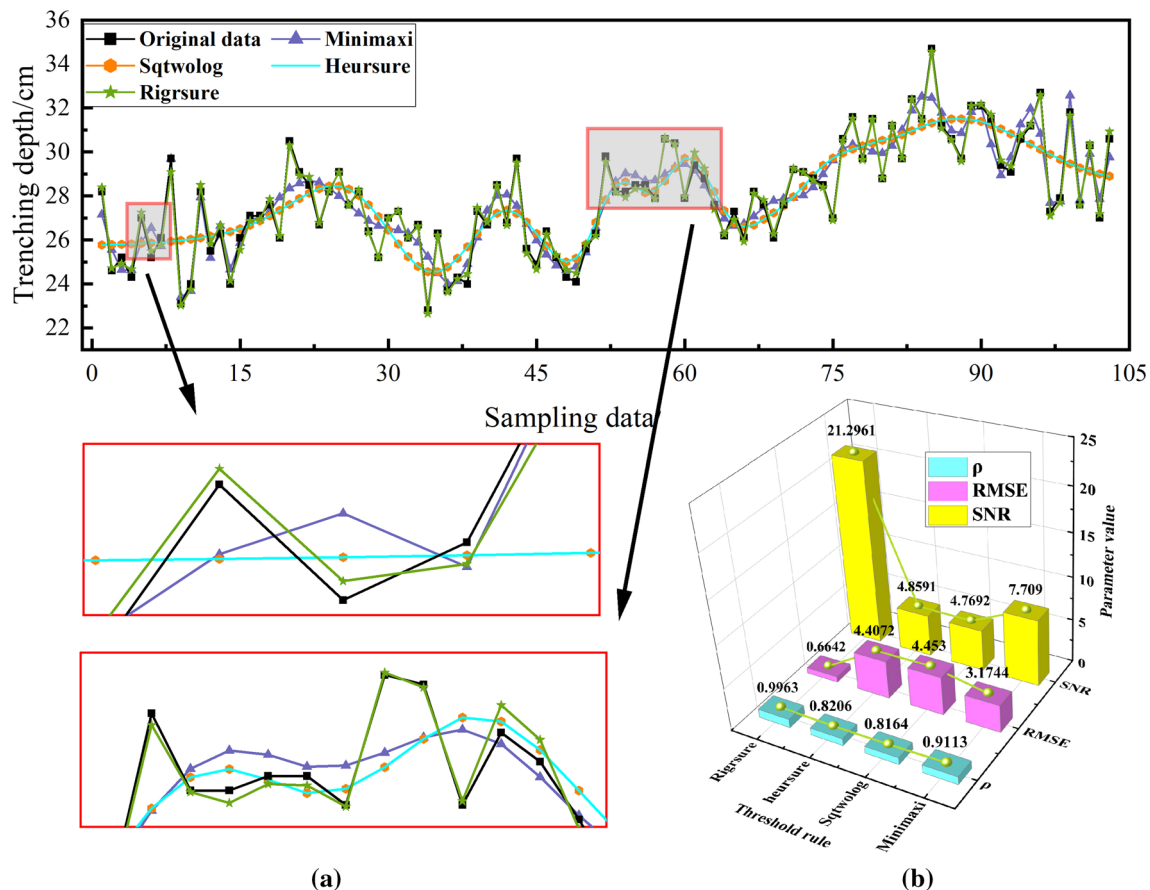


**Fig. 8** Data noise reduction performance under different threshold rules

select the threshold method to improve the performance of the wavelet denoising preprocessing part of the trenching depth data.

Under the wavelet parameter combination of wavelet function db9, four-level wavelet decomposition, and hard threshold function, four different threshold rules are selected to denoise the data respectively, namely Sqtwolog, Rigrsure, Heursure, and Minimaxi. Comparing and analyzing their noise reduction performance, the results are shown in Fig. 8.

Corresponding to Fig. 8a, it can be noticed that the data processed by Sqtwolog and Heursure threshold rules are very similar and smooth, while the data processed by Rigrsure and Minimax threshold rules are relatively rough. Simultaneously, combined with the local magnified images, we can find that in the processing results of the two selected pieces of data, the data after Sqtwolog and Heursure thresholding rules are too smooth, resulting in serious signal distortion. Although the data waveform processed by the Minimax threshold rule can be similar to the changing trend of the original data compared with the processing results of the Sqtwolog and Heursure threshold rules, unfortunately, as can be seen in the second partial enlarged image, the Minimax threshold rule also produces relatively severe signal distor-

**Table 6** Evaluation indexes of wavelet noise reduction performance under different threshold rules

Threshold rule	Minimaxi	Sqtwolog	Heursure	Rigrsure
SNR	7.7090	4.7692	4.8591	21.2961
RMSE	3.1744	4.4530	4.4072	0.6642
$\rho$	0.9113	0.8164	0.8206	0.9963

tion. The severe distortion caused by these threshold rules will greatly reduce the performance of the wavelet noise reduction algorithm, which can also be analyzed from Fig. 8b and Table 6.

#### 4.5 Pretreatment of Trenching Depth

Hence, the threshold rule ‘‘Rigrsure’’, decomposition Level 4, and the wavelet function ‘‘db9’’ are the preferred parameters during the wavelet noise reduction preprocessing part for trenching depth data. Under this combination, noise reduction is performed on the original trenching depth data at three depth levels of 25 cm, 30 cm, and 35 cm, and the trenching depth data before and after noise reduction are shown in Fig. 9.



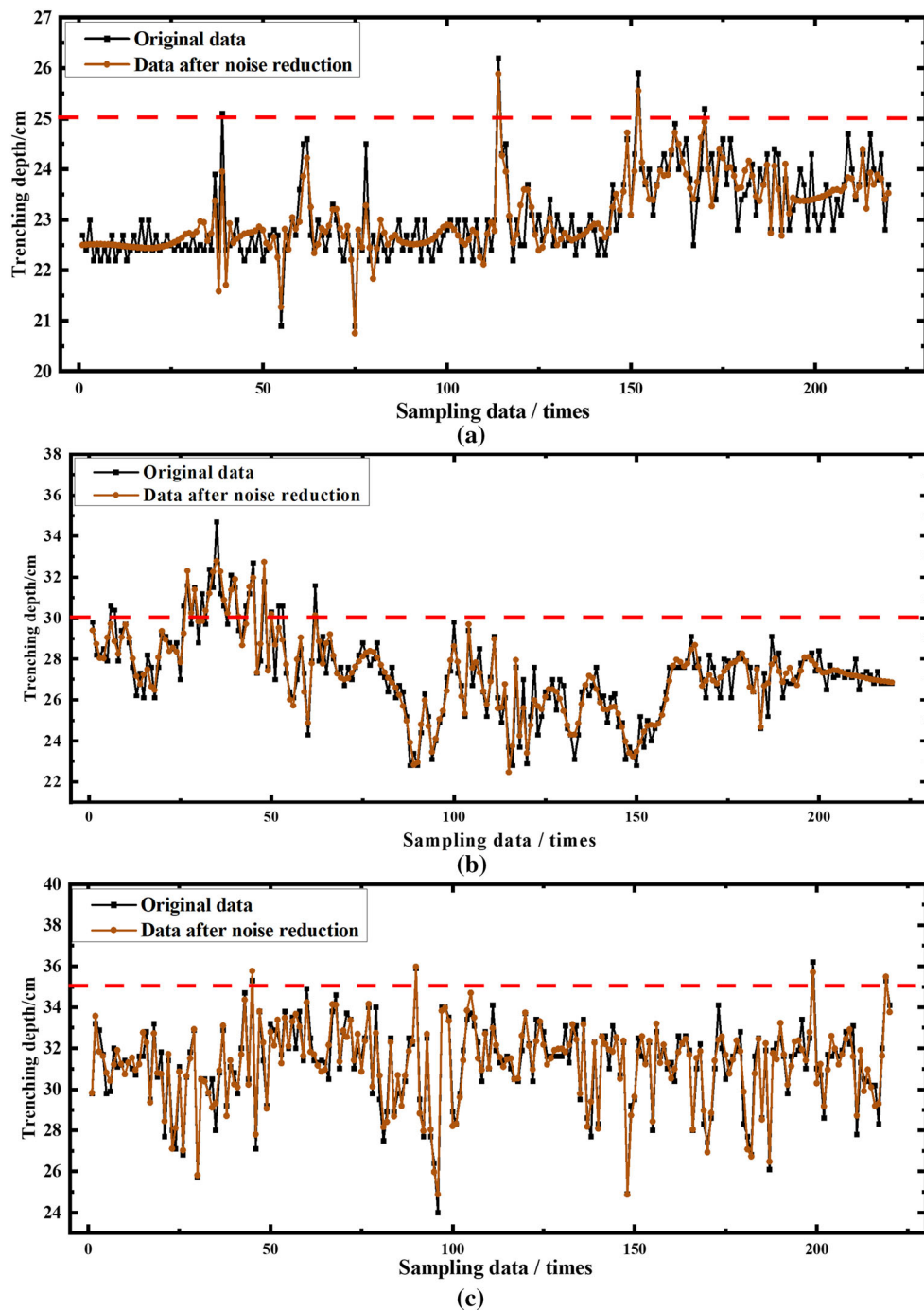


**Fig. 9** Data after wavelet noise reduction

When using the wavelet noise reduction preprocessing part under the optimal parameters combination to process the data noise, it can effectively remove the noise while retaining the data characteristics, so that the monitoring data after noise reduction is closer to the truth value. The mean, variance, and mean square error of the data before and after wavelet preprocessing are shown in Table 7 and Fig. 10.

As the depth level increases from small to large, in the preprocessed local data, the mean value decreases by 0.015 cm,

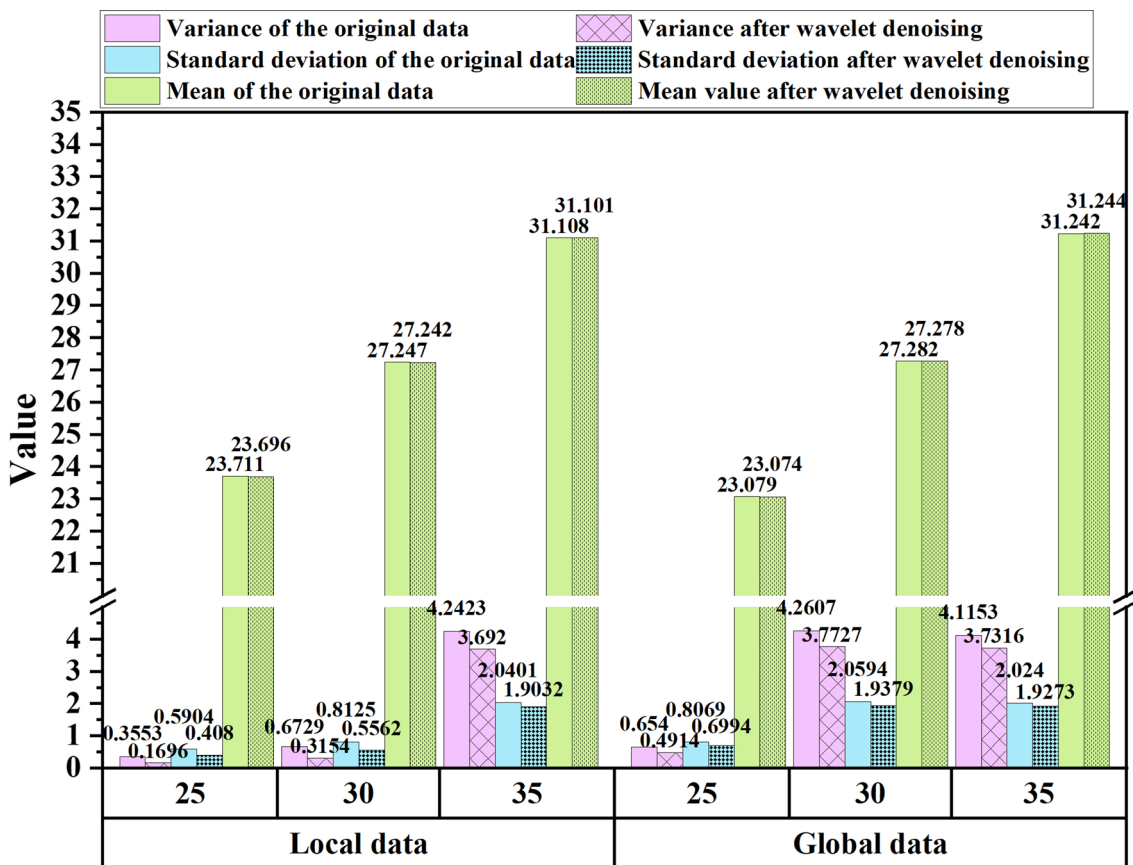
0.005 cm, and 0.007 cm, and the variance decreases by 0.1857, 0.3575, and 0.5503, respectively. Simultaneously, the mean squared error decreased by 0.1824, 0.2563, and 0.1369, respectively. In the preprocessed global data, the mean value is reduced by 0.005 m, 0.004 cm, -0.002 cm, the variance is reduced by 0.1626, 0.488, and 0.3837, and the mean square error is reduced by 0.1075, 0.1215, and 0.0967.

To sum up, whether it is local data or global data, the data mean has not changed obviously, but the variance and



**Table 7** Mean, variance, and mean square error results before and after preprocessing

Depth level/cm	Mean of the original data		Mean value after wavelet denoising		Variance of the original data		Variance after wavelet denoising		Standard deviation of the original data		Standard deviation after wavelet denoising	
	Local data	Global data	Local data	Global data	Local data	Global data	Local data	Global data	Local data	Global data	Local data	Global data
25	23.711	23.079	23.696	23.074	0.3553	0.654	0.1696	0.4914	0.5904	0.8069	0.408	0.6994
30	27.247	27.282	27.242	27.278	0.6729	4.2607	0.3154	3.7727	0.8125	2.0594	0.5562	1.9379
35	31.108	31.242	31.101	31.244	4.2423	4.1153	3.692	3.7316	2.0401	2.024	1.9032	1.9273

**Fig. 10** Comparison of data mean, variance, and mean square error before and after preprocessing

standard deviation of the data have been reduced to a certain extent. This also proves that the work in Sect. 4 is of great significance for denoising the original data.

estimated value of the current moment. The recursion is performed in the order of "measurement-prediction-correction" to minimize the impact of noise on the system. The processing flow is shown in Fig. 11.

In this monitoring system, due to the short time interval of trenching depth data collection, we usually assume that the trenching depth at the current moment is the same as the trenching depth at the previous moment, so the gain of the current state is  $I = 1$ . Since there is no control parameter in the filtering process of trench depth, so  $I = 1$ . The actual trenching depth data correspond directly to the trenching depth measurements, so  $I = 1$ .  $Q$  is the state noise covariance, and  $R$  is the observation noise covariance. In the correction part,

## 5 Kalman Filter Reprocessing Part

### 5.1 The Principle of Kalman Filter

The Kalman filter algorithm uses the state-space model of signal and noise, updates the estimated value of the state variable through the estimated value of the previous moment and the observed value of the current moment, and calculates the



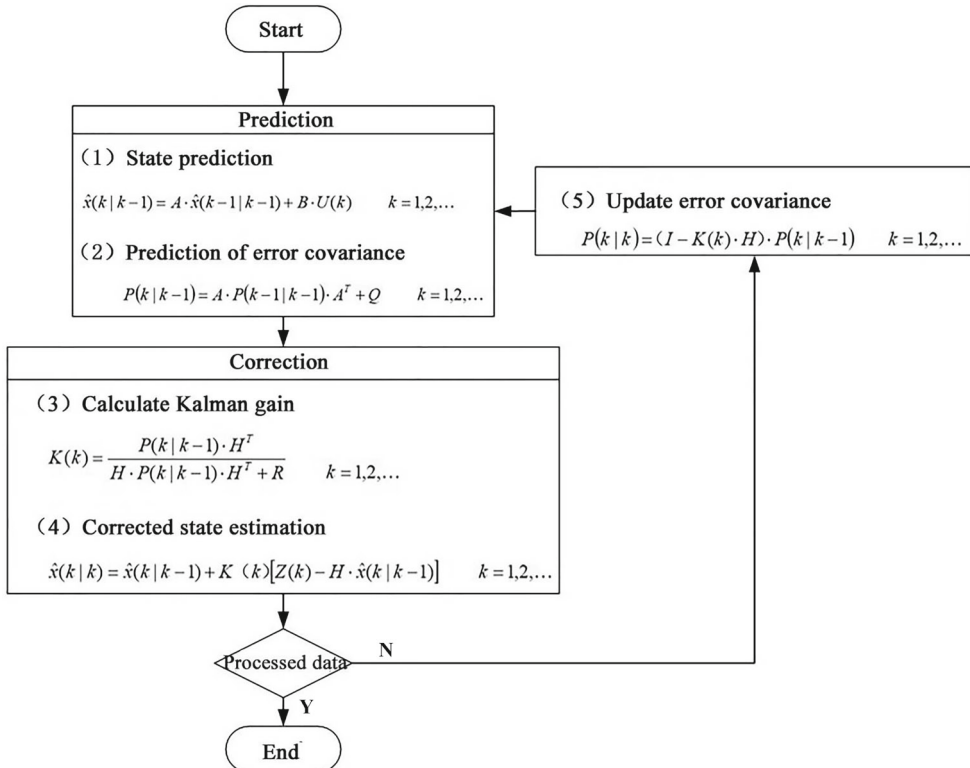


**Fig. 11** Kalman filter processing flow

the optimal gain will change with the change of  $Q$  and  $R$ , so different  $Q$  and  $R$  values will form different filtering effects. To further explore the effect of  $Q$  and  $R$  values on the performance of the reprocessing part of the Kalman filter applied to trench depth data, we will explore the optimal  $Q/R$  ratio and the optimal  $Q/R$  combination under a fixed  $Q/R$  ratio.

## 5.2 Simulation Analysis

At the depth level of 35 cm, the mean, variance and standard deviation of the data presented the worst quality, so the original trenching depth data at the 35 cm level was used in this subsection as the experimental data. First, this paper assumes the parameters  $Q$  and  $R$  to be constants. By setting different parameter combinations, Kalman filtering is performed on the above trenching depth data. The value of  $R$  is set as  $R = 2$ ; the value of  $Q$  is taken as  $Q = 4$ ,  $Q = 2$ ,  $Q = 0.2$ ,  $Q = 0.02$ ,  $Q = 0.002$ , respectively; to explore the filtering effect under different  $Q/R$  ratios, the filtering effect diagram is shown in Fig. 12.

Figure 12 shows that the overall data trends after filtering are similar under different  $Q/R$  ratio parameters. However, a higher  $Q/R$  value has a poor filtering effect on data with severe fluctuations, and the overall filtering quality is not good. With the decrease of the  $Q/R$  value, the filtering quality

is gradually improved, and it has a better filtering effect on abnormally fluctuating data.

Combining Fig. 12f and Table 8 concurrently, it can be seen that with the decrease of  $Q/R$ , the mean value of the data is getting closer and closer to the set depth level. After filtering, the variance and standard deviation gradually decrease, showing a sharp decrease trend first and then a gentle decrease. Finally, when the  $Q/R$  ratio is 0.1, the decreasing trend is stable step by step. Through analysis and comparison, it can be noticed that when the  $Q/R$  value is 0.001 Kalman filter works best.

In the case where the  $Q/R$  ratio is 0.001, four combinations are set in this paper: (1)  $R = 1$ ,  $Q = 0.001$ . (2)  $R = 2$ ,  $Q = 0.002$ . (3)  $R = 3$ ,  $Q = 0.003$ . (4)  $R = 4$ ,  $Q = 0.004$ . Under a fixed  $Q/R$  ratio, this subsection explores the optimal parameter combination for  $Q$  and  $R$  in more depth. The filtering results are shown in Table 9.

The corresponding filtering results and result comparison are shown in Fig. 13.

The results show that under a fixed  $Q/R$  value, with the decreasing value of  $Q$  and the increasing value of  $R$ , the mean difference is getting closer to its depth level, and the variance and standard deviation are decreasing. When the parameter combination is  $R = 3$ ,  $Q = 0.003$ , the increasing trend of the mean slows down, but the variance decreases to half of that under the combination of  $R = 2$ ,  $Q = 0.002$ , indicating that



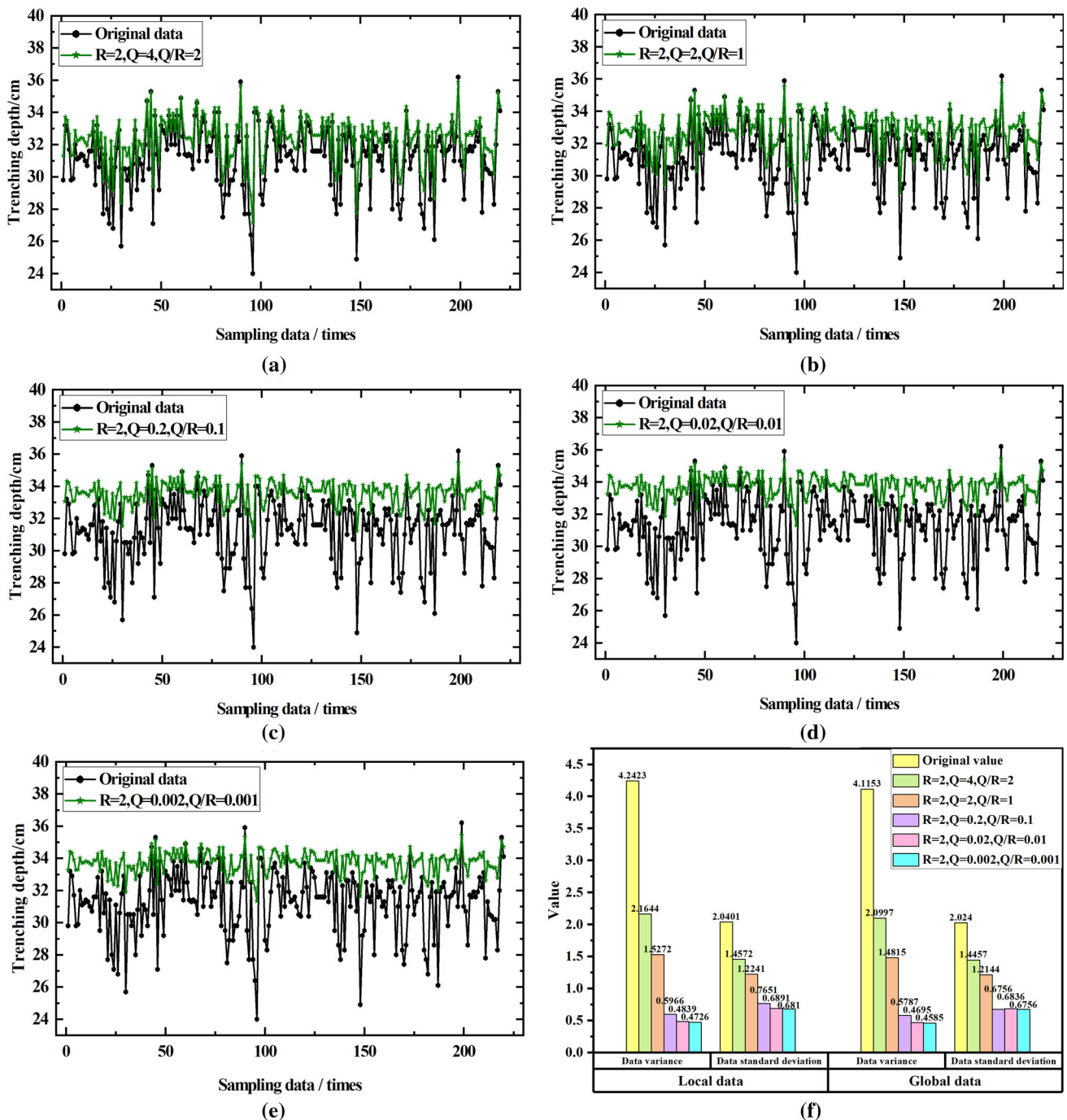


**Fig. 12** The effect of Kalman filter under different Q/R ratios

under the combination of  $R = 3, Q = 0.003$ , The degree of dispersion of the filtered data becomes smaller.

Combining with Fig. 13a, it can also be found that the fluctuation of the filtered data becomes smoother and smoother. It can be seen from the two partially enlarged images that under the two combinations of  $R = 3, Q = 0.003$  and  $R = 4, Q = 0.004$ , the data is too smooth and cause relatively serious

data distortion. The situations described above are reflected in local data and global data.

Therefore, the value combination of the algorithm parameters of the Kalman filter reprocessing part finally selected in this section is  $R = 2, Q = 0.002$ .



**Table 8** The mean, variance, and standard deviation of the filtered data at different Q/R values

Group		Local data								
		R	Q	Q/R	Variance of the original data	Variance of the filtered data	Standard deviation of the original data	Standard deviation of the filtered data	Mean of the original data	Mean of the filtered data
1	2	0.002	0.001	4.2423		0.4726	2.0401	0.6810	31.108	33.701
2	2	0.02	0.01			0.4839		0.6891		33.685
3	2	0.2	0.1			0.5966		0.7651		33.540
4	2	2	1			1.5272		1.2241		32.665
5	2	4	2			2.1644		1.4572		32.220
Group		Global data								
		R	Q	Q/R	Variance of the original data	Variance of the filtered data	Standard deviation of the original data	Standard deviation of the filtered data	Mean of the original data	Mean of the filtered data
1	2	0.002	0.001	4.1153		0.4585	2.0240	0.6756	31.242	33.746
2	2	0.02	0.01			0.4695		0.6836		33.731
3	2	0.2	0.1			0.5787		0.7590		33.591
4	2	2	1			1.4815		1.2144		32.745
5	2	4	2			2.0997		1.4457		32.316

**Table 9** Mean, variance, and standard deviation of filtered data at different Q and R values

Group		Local data			
		R	Q	Variance of the filtered data	Standard deviation of the filtered data
1	1	0.001		1.0616	1.0206
2	2	0.002		0.4726	0.6810
3	3	0.003		0.2663	0.5112
4	4	0.004		0.1708	0.4093
Group		Global data			
		R	Q	Variance of the filtered data	Standard deviation of the filtered data
1	1	0.001		1.0299	1.0125
2	2	0.002		0.4585	0.6756
3	3	0.003		0.2584	0.5071
4	4	0.004		0.1657	0.4061

## 6 Application and analysis

In summary, all parameters in this paper have been determined. The parameters of the wavelet preprocessing part are the wavelet basis function db9, the decomposition level is 4, the optimal threshold rule is Rigrsure, and the parameters of the Kalman filter reprocessing part are selected as  $R = 2$ ,  $Q = 0.002$ . According to the comprehensive algorithm processing flow described in Sect. 3, this paper performs filtering and noise reduction processing on the trenching depth data collected by the monitoring system at three depth levels of 25 cm, 30 cm, and 35 cm. The filtered data are shown in Fig. 14.

According to Fig. 14, it can be found that both the Kalman filter algorithm and the comprehensive noise reduction correction algorithm have a good noise reduction and correction performance for the original trenching data. However, compared with the two filtering algorithms, it can be found that, compared with the Kalman filtering algorithm, the comprehensive noise reduction correction algorithm proposed in this paper can not only eliminate data noise, suppress data jitter, and correct data, but also make the data maintain the original trend of change. This is because when the Kalman filter algorithm is used, the noise is assumed to be Gaussian white noise, but the noise component in the actual trenching process is more complicated, and the assumption conditions of the



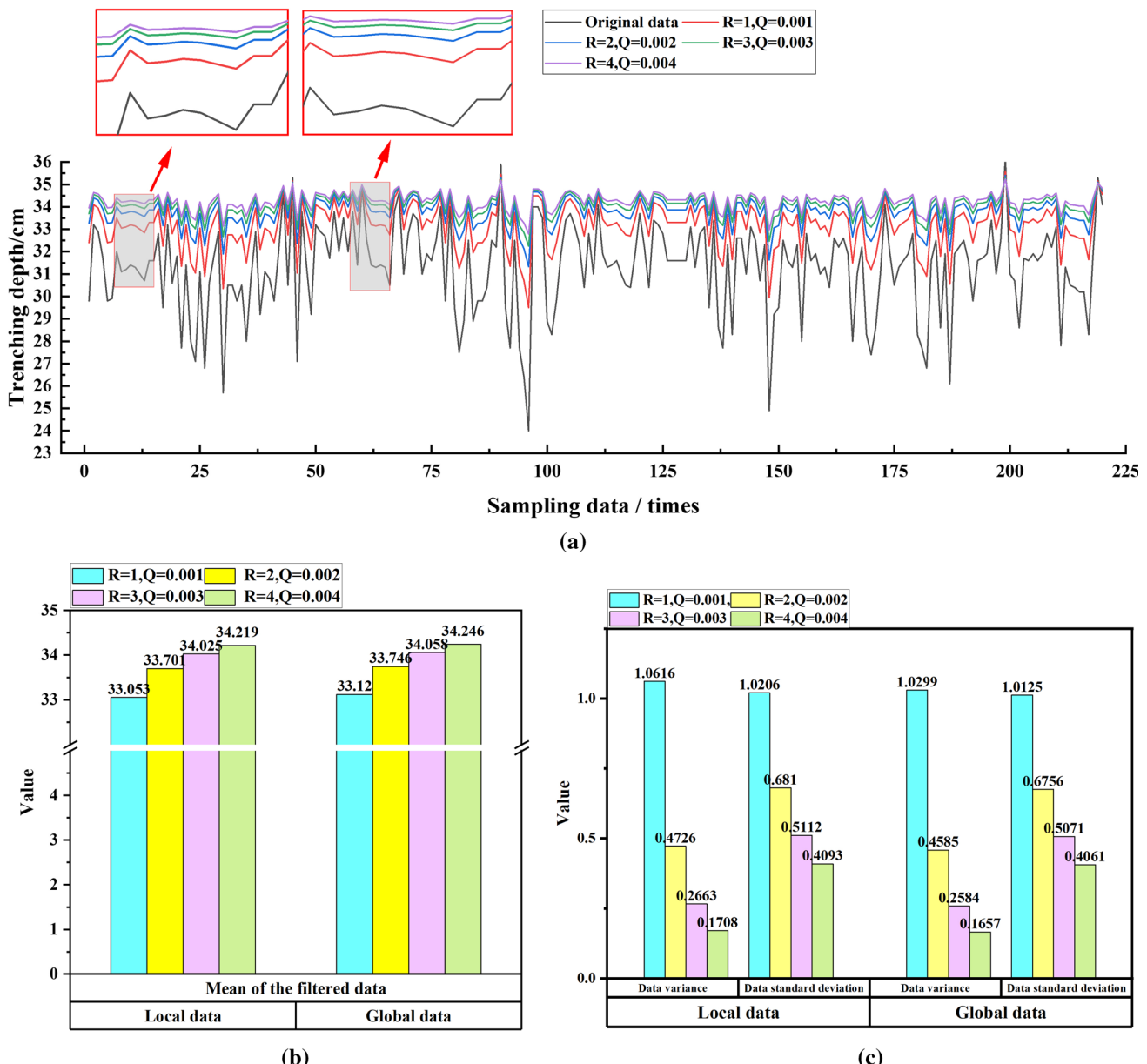


**Fig. 13** Schematic diagram of filtering results and comparison under different Q and R values

Kalman filter cannot be well satisfied. The wavelet denoising preprocessing part introduced in this algorithm can eliminate the data noise and provide data with better precision for the subsequent Kalman reprocessing part.

The data processed by the two processing algorithms are shown in Table 10 and Fig. 15. Among them, in the local data and the global data, the average value of the trenching depth data processed by the two algorithms is very close. The difference is that the performance of the comprehensive algorithm is better than that of the Kalman filter algorithm in terms of variance and standard deviation, which further shows that the comprehensive algorithm has better perfor-

mance in noise reduction and correction of trenching depth data.

The performance of the synthetic filter correction algorithm and the single Kalman filter algorithm is compared and analyzed. By comparing the data processing results of the two algorithms, we found that for local data, the variance decreased by 0.0207, 0.0398, and 0.0609, and the mean square deviation decreased by 0.0609, 0.0854, and 0.0457. The mean of the two algorithms did not change significantly. Likewise, for the global data, the variance drops by 0.0182, 0.0549, 0.0428, and the mean square deviation drops by 0.0359, 0.041, 0.0323.



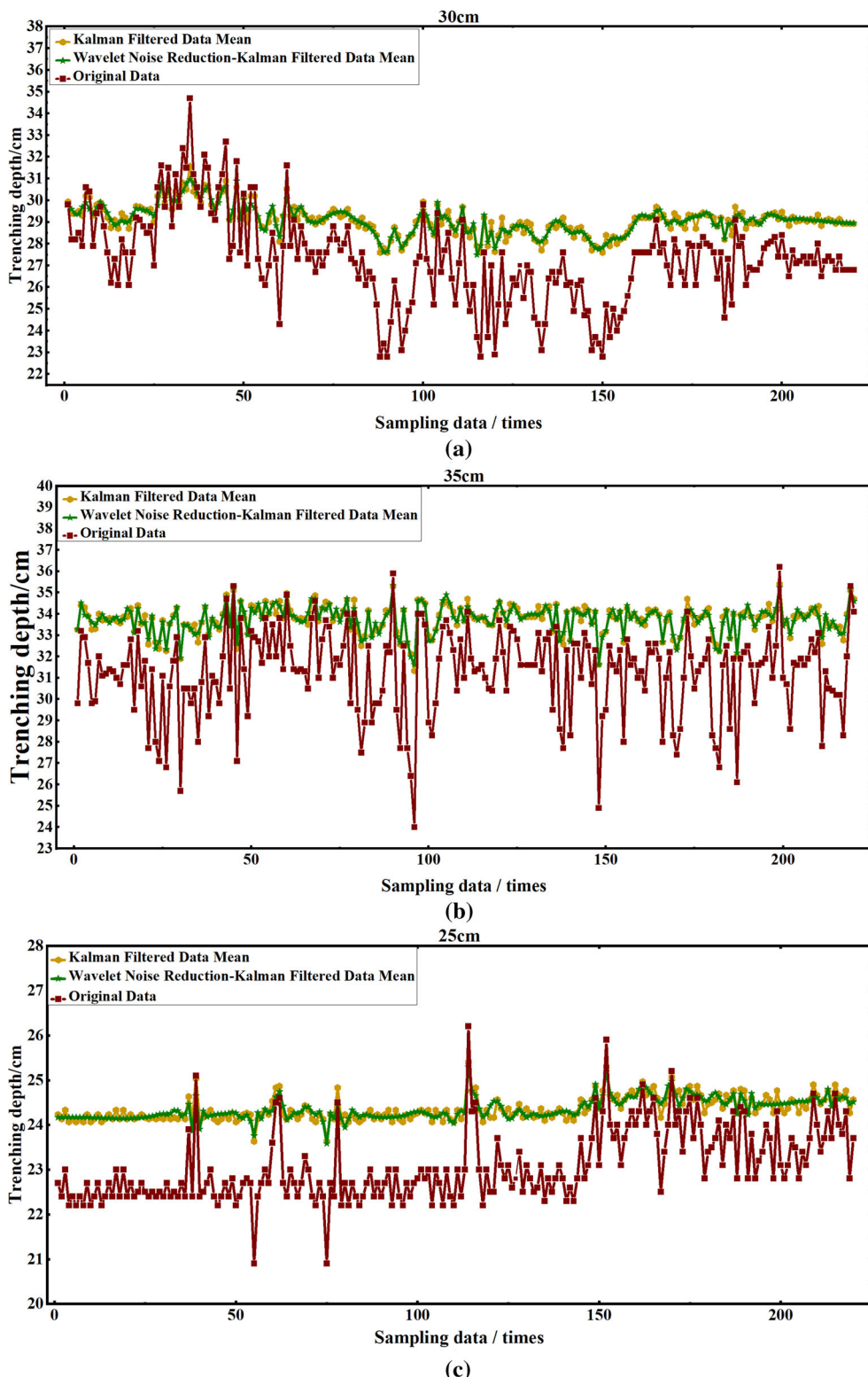


**Fig. 14** Data processed by a comprehensive algorithm

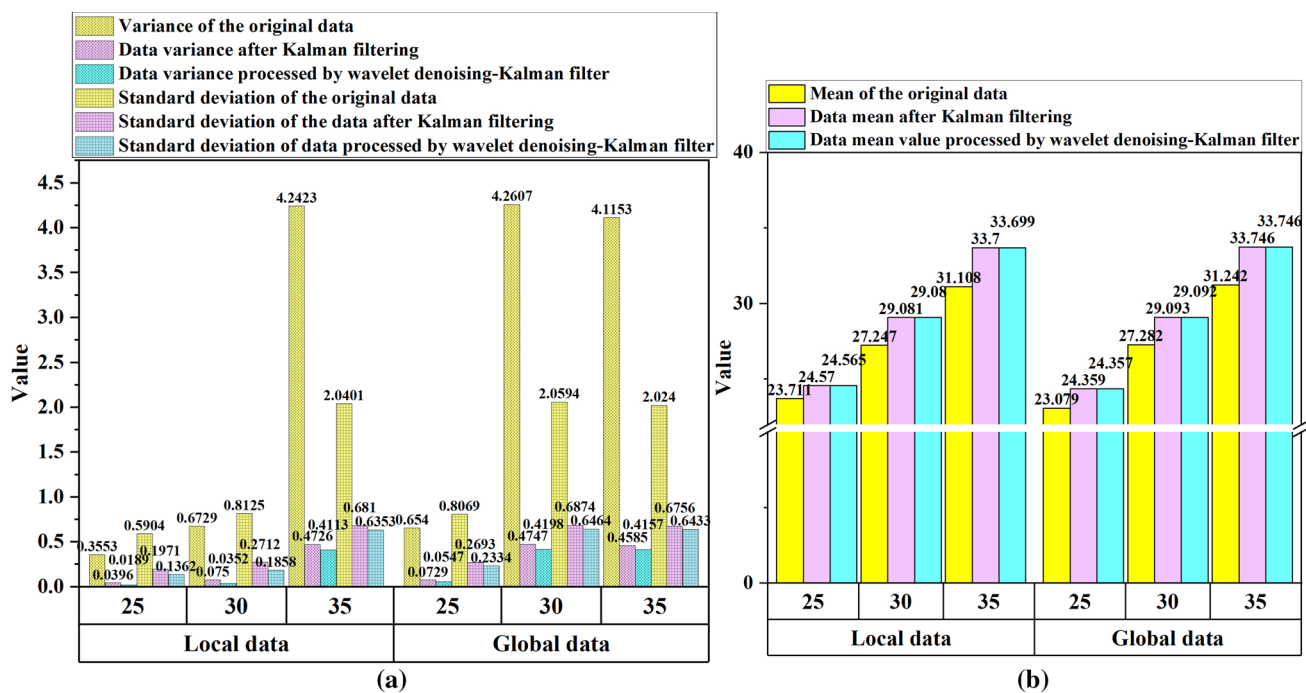
To sum up, compared with the data processed by the Kalman filter algorithm, the data processed by the comprehensive correction algorithm has no significant change in

the mean value. Nevertheless, the data variance and standard deviation results processed by the comprehensive algorithm are lower, and this phenomenon exists in both local and global



**Table 10** Mean, variance, and standard deviation after different filtering methods

Depth level/cm	Mean of the original data		Data mean after Kalman filtering		Data mean value processed by wavelet denoising-Kalman filter	
	Local data	Global data	Local data	Global data	Local data	Global data
25	23.711	23.079	24.570	24.359	24.565	24.357
30	27.247	27.282	29.081	29.093	29.080	29.092
35	31.108	31.242	33.700	33.746	33.699	33.746
Depth level/cm	Variance of the original data		Data variance after Kalman filtering		Data variance processed by wavelet denoising-Kalman filter	
	Local data	Global data	Local data	Global data	Local data	Global data
25	0.3553	0.6540	0.0396	0.0729	0.0189	0.0547
30	0.6729	4.2607	0.0750	0.4747	0.0352	0.4198
35	4.2423	4.1153	0.4726	0.4585	0.4113	0.4157
Depth level/cm	Standard deviation of the original data		Standard deviation of the data after Kalman filtering		Standard deviation of data processed by wavelet denoising-Kalman filter	
	Local data	Global data	Local data	Global data	Local data	Global data
25	0.5904	0.8069	0.1971	0.2693	0.1362	0.2334
30	0.8125	2.0594	0.2712	0.6874	0.1858	0.6464
35	2.0401	2.0240	0.6350	0.6464	0.6433	0.6433

**Fig. 15** Comparison of mean, variance, and standard deviation after different filtering methods

data. It shows that the comprehensive algorithm is better than the single Kalman filter algorithm in performance and has better processing quality in both local and global data.

## 7 Conclusions

In this paper, we propose a wavelet noise reduction-Kalman filter trenching depth correction algorithm, which consists of a wavelet noise reduction preprocessing part and a Kalman



filter reprocessing part. By comprehensively processing the local data and global data of the trenching depth, the algorithm realizes the comprehensive noise reduction and correction of the data. This paper considers the interaction between the performance of wavelet denoising preprocessing part and the parameters combination of wavelet functions, decomposition level, and thresholding rule. The article also discusses the influence of Kalman filter Q/R parameters and the combination of Q and R parameters on the quality of data reprocessing. It is proved that the processing quality of the comprehensive algorithm in both local and global data is higher than that of the single Kalman filter algorithm. The work of this paper is summarized as follows:

- (1) To maximize the performance of the preprocessing part of wavelet noise reduction, Sect. 4 determines the optimal parameter combination of the preprocessing part. Considering the noise reduction performance and calculation amount, the optimal parameters combination of the wavelet noise reduction preprocessing part is determined as db9 wavelet basis function, four-level decomposition level, and Rigrsure threshold rule. The wavelet denoising preprocessing part under this parameter combination processes the sample data. There is no obvious difference between the local data and the global data in the mean, but the comprehensive algorithm both reduce the variance and standard deviation of the data. Hence, the wavelet noise reduction part under the optimal parameter combination has an essential influence on improving data quality and reducing data noise.
- (2) To find a balance between data filtering and distortion in the reprocessing part of the Kalman filter, the performance effects of different Q/R values and different combinations of Q and R parameters on the performance of the Kalman filter reprocessing part are compared and analyzed. After filtering, the variance and standard deviation gradually decrease, showing a sharp decrease trend first and then a gentle decrease. Finally, when the Q/R ratio is 0.1, the decreasing trend is stable step by step, and its filtering effect is also the best. Under a fixed Q/R value, with the decreasing value of Q and the increasing value of R, the mean difference is getting closer to its depth level, and the variance and standard deviation are decreasing. When the parameter combination is  $R = 3$ ,  $Q = 0.003$ , the data is too smooth and causes relatively serious data distortion. Therefore, the value combination of the algorithm parameters of the Kalman filter reprocessing part finally selected in this section is  $R = 2$ ,  $Q = 0.002$ .
- (3) To test the feasibility and advantages of the comprehensive algorithm in data processing, the ditching depth data at three levels of 25 cm, 30 cm, and 35 cm were verified and processed. Compared with the data processed

by the Kalman filter algorithm, the data processed by the comprehensive correction algorithm has no significant change in the mean value. Nevertheless, the data variance and standard deviation results processed by the comprehensive algorithm are lower, and this phenomenon exists in both local and global data. It shows that the comprehensive algorithm is better than the single Kalman filter algorithm in performance, and has better processing quality in both local and global data.

- (4) To verify the processing performance of the algorithm in local and global data, the performance of the synthetic filter correction algorithm and the single Kalman filter algorithm is compared and analyzed. By comparing the data processing results of the two algorithms, we found that for local data, the variance decreased by 0.0207, 0.0398, and 0.0609, and the mean square deviation decreased by 0.0609, 0.0854, and 0.0457. The mean of the two algorithms did not change significantly. Likewise, for the global data, the variance drops by 0.0182, 0.0549, and 0.0428, and then the mean square deviation drops by 0.0359, 0.041, and 0.0323.

In future research work, we will further explore the impact of operation environment, soil characteristics, equipment operation status, system design, and data quality. According to the noise characteristics generated by different factors, we will establish different parameter models and filtering algorithms and add artificial neural network algorithms to improve the reliability and robustness of the monitoring system and provide a reliable data source for subsequent operation quality identification and operation control judgment.

**Funding** This study was financially supported by the Central government guides local technology development funds of China (Grant No. KC005103) and Domain Development Corps division Innovation Support Program of China (Grant No. 2018BB042) and National Natural Science Foundation of China (Grant No. 32060417).

## Declarations

**Conflict of interest** The authors declare no conflict of interest.

## References

1. Zhao, C.; Gao, B.; Wang, L.; Huang, W.; Xu, S.; Cui, S., Spatial patterns of net greenhouse gas balance and intensity in Chinese orchard system. *Sci. Total Environ.* 779 (2021)
2. FAO, 2020. Statistical database of the food and agriculture organization of the United Nations. available at. <https://www.fao.org/faostat/en/#data/QCL>.
3. Hansson, L.J.; Ring, E.; Franko, M.A.; Gärdenäs, A.I.: Soil temperature and water content dynamics after disc trenching a sub-xeric



- Scots pine clearcut in central Sweden. *Geoderma* **327**, 85–96 (2018)
4. Ma, C.; Qi, J.T.; Kan, Z.; Chen, S.J.; Meng, H.W.: Operation power consumption and verification tests of a trenching device for orchards in Xinjiang based on discrete element. *Int. J. Agric. Biol. Eng.* **14**(1), 133–141 (2021)
  5. Ersson, B.T.; Cormier, D.; St-Amour, M.; Guay, J.: The impact of disc settings and slash characteristics on the Bracke three-row disc trencher's performance. *Int. J. For. Eng.* **28**(1), 1–9 (2017)
  6. Ring, E.; Hogbom, L.; Jacobson, S.; Jansson, G.; Nohrstedt, H.O.: Long-term effects on soil-water nitrogen and pH of clearcutting and simulated disc trenching of previously nitrogen-fertilised pine plots (vol 48, pg 1115, 2018). *Can. J. For. Res.* **51**(10), 1579–1579 (2021)
  7. Martins, R. N.; Fagundes Portes, M.; Fialho e Moraes, H. M.; Ribeiro Furtado Junior, M.; Fim Rosas, J. T.; Orlando Junior, W. d. A., Influence of tillage systems on soil physical properties, spectral response and yield of the bean crop. *Remote Sens. Appl.: Soc. Environ* **22** (2021)
  8. Toselli, M.; Baldi, E.; Cavani, L.; Mazzon, M.; Quartieri, M.; Sorrenti, G.; Marzadori, C.: Soil-plant nitrogen pools in nectarine orchard in response to long-term compost application. *Sci. Total Environ.* **671**, 10–18 (2019)
  9. Zheng, W.; Gong, Q.; Lv, F.; Yin, Y.; Li, Z.; Zhai, B.: Tree-scale spatial responses of extracellular enzyme activities and stoichiometry to different types of fertilization and cover crop in an apple orchard. *Eur. J. Soil Biol.* **99** (2020)
  10. Xiang, Y.; Li, Y.; Liu, Y.; Zhang, S.; Yue, X.; Yao, B.; Xue, J.; Lv, W.; Zhang, L.; Xu, X.; Li, Y.; Li, S.: Factors shaping soil organic carbon stocks in grass covered orchards across China: A meta-analysis. *Sci. Total Environ.* **807** (2022)
  11. Jia, H.; Guo, M.; Yu, H.; Li, Y.; Feng, X.; Zhao, J.; Qi, J.: An adaptable tillage depth monitoring system for tillage machine. *Biosys. Eng.* **151**, 187–199 (2016)
  12. Nielsen, S.K.; Nørremark, M.; Green, O.: Sensor and control for consistent seed drill coulter depth. *Comput. Electron. Agric.* **127**, 690–698 (2016)
  13. Nielse, S.K.; Munkholm, L.J.; Lamande, M.; Norremark, M.; Edwards, G.T.C.; Green, O.: Seed drill depth control system for precision seeding. *Comput. Electron. Agric.* **144**, 174–180 (2018)
  14. Wang, Y.; Zhang, D.; Yang, L.; Cui, T.; Zhang, W.; Qi, B.; Li, Y.; Zhong, X.: Field performance of an electric-hydraulic control system for vibrating subsoiler with flexible tines. *Comput. Electron. Agric.* **172**, 105377 (2020)
  15. Shafaei, S.M.; Loghavi, M.; Kamgar, S.: A practical effort to equip tractor-implement with fuzzy depth and draft control system. *Eng. Agricul., Environ. Food* **12**(2), 191–203 (2019)
  16. Soylu, S.; Çarman, K.: Fuzzy logic based automatic slip control system for agricultural tractors. *J. Terramech.* **95**, 25–32 (2021)
  17. Quan, X.; Lv, H.; Liu, C.; Wang, H.; Wu, D.; Chen, P.; Zhou, H.: An investigation on bolt stress ultrasonic measurement based on acoustic time difference algorithm with adaptive hybrid extended Kalman filter. *Measurement* **186** (2021)
  18. Namdar, A.; Samet, H.; Allahbakhshi, M.; Tajdinian, M.; Ghanbari, T.: A robust stator inter-turn fault detection in induction motor utilizing Kalman filter-based algorithm. *Measurement* **187**, 110181 (2022)
  19. Jiang, H.; Liu, G.; Li, J.; Zhang, T.; Wang, C.; Ren, K.: Model based fault diagnosis for drillstring washout using iterated unscented Kalman filter. *J. Petrol. Sci. Eng.* **180**, 246–256 (2019)
  20. Hu, G.; Gao, B.; Zhong, Y.; Gu, C.: Unscented kalman filter with process noise covariance estimation for vehicular ins/gps integration system. *Information Fusion* **64**, 194–204 (2020)
  21. Li, S.; Zhang, M.; Ji, Y.; Zhang, Z.; Cao, R.; Chen, B.; Li, H.; Yin, Y.: Agricultural machinery GNSS/IMU-integrated navigation based on fuzzy adaptive finite impulse response Kalman filtering algorithm. *Comput. Electron. Agric.* **191**, 106524 (2021)
  22. Yu, Z.; Yang, K.; Luo, Y.; Shang, C.: Spatial-temporal process simulation and prediction of chlorophyll-a concentration in Dianchi Lake based on wavelet analysis and long-short term memory network. *J. Hydrol.* **582**, 124488 (2020)
  23. Gurav, M.; Sarik, S.; Singh, K.; Pendharkar, G.; Shojaei Baghini, M.: IITB\_TDR: A portable TDR system with DWT based denoising for soil moisture measurement. *Sens. Actuators, A* **283**, 317–329 (2018)
  24. Alhnaity, B.; Kollias, S.; Leontidis, G.; Jiang, S.; Schamp, B.; Pearson, S.: An autoencoder wavelet based deep neural network with attention mechanism for multi-step prediction of plant growth. *Inf. Sci.* **560**, 35–50 (2021)
  25. Lin, D.; Li, G.; Zhu, Y.; Liu, H.; Li, L.; Fahad, S.; Zhang, X.; Wei, C.; Jiao, Q.: Predicting copper content in chicory leaves using hyperspectral data with continuous wavelet transforms and partial least squares. *Comput. Electron. Agric.* **187**, 106293 (2021)
  26. Katunin, A.; Aratijo dos Santos, J.V.; Lopes, H.: Damage identification by wavelet analysis of modal rotation differences. *Structures* **30**, 1–10 (2021)
  27. Li, J.; Wang, H.; Wang, X.; Zhang, Y.: Rolling bearing fault diagnosis based on improved adaptive parameterless empirical wavelet transform and sparse denoising. *Measurement* **152**, 107392 (2020)
  28. Gu, J.; Yang, T.S.; Ye, J.C.; Yang, D.H.: CycleGAN denoising of extreme low-dose cardiac CT using wavelet-assisted noise disentanglement. *Med. Image Anal.* **74**, 102209 (2021)
  29. Pouyani, M.F.; Vali, M.; Ghasemi, M.A.: Lung sound signal denoising using discrete wavelet transform and artificial neural network. *Biomed. Signal Process. Control* **72**, 103329 (2022)
  30. Gungor, M. A., A comparative study on wavelet denoising for high noisy CT images of COVID-19 disease. *Optik* **235** (2021)
  31. Peng, S.; Chen, R.; Yu, B.; Xiang, M.; Lin, X.; Liu, E.: Daily natural gas load forecasting based on the combination of long short term memory, local mean decomposition, and wavelet threshold denoising algorithm. *J. Natural Gas Sci. Eng.* **95**, 104175 (2021)
  32. Pan, L.; Chen, Y.; Xu, Y.; Li, J.; Lu, H., A model for soil moisture content prediction based on the change in ultrasonic velocity and bulk density of tillage soil under alternating drying and wetting conditions. *Measurement* **110504** (2021)
  33. Huang, S.; Lu, C.; Li, H.; He, J.; Wang, Q.; Yuan, P.; Gao, Z.; Wang, Y.: Transmission rules of ultrasonic at the contact interface between soil medium in farmland and ultrasonic excitation transducer. *Comput. Electron. Agric.* **190**, 106477 (2021)
  34. Huimin, C.U.I.; Ruimei, Z.; Yanli, H.O.U.: Improved Threshold Denoising Method Based on Wavelet Transform. *Phys. Procedia* **33**, 1354–1359 (2012)
  35. Li, Z.C.; Wang, T.Z.; Wang, Y.D.; Amarat, Y.; Benbouzid, M.; Diallo, D.: A Wavelet Threshold Denoising-Based Imbalance Fault Detection Method for Marine Current Turbines. *IEEE ACCESS* **8**, 29815–29825 (2020)
  36. Kumar, A.; Tomar, H.; Mehla, V.K.; Komaragiri, R.; Kumar, M.: Stationary wavelet transform based ECG signal denoising method. *ISA Trans.* **114**, 251–262 (2021)

